Chemical Science

ROYAL SOCIETY OF CHEMISTRY

EDGE ARTICLE

View Article Online
View Journal | View Issue

Cite this: *Chem. Sci.*, 2020, **11**, 3996

All publication charges for this article have been paid for by the Royal Society of Chemistry

Synthesis, conformational analysis and *in vivo* assays of an anti-cancer vaccine that features an unnatural antigen based on an sp^2-iminosugar fragment†

Iris A. Bermejo,[a] Claudio D. Navo,[ab] Jorge Castro-López,[c] Ana Guerreiro,[d] Ester Jiménez-Moreno,[a] Elena M. Sánchez Fernández,[e] Fayna García-Martín,[f] Hiroshi Hinou,[f] Shin-Ichiro Nishimura,[f] José M. García Fernández,[g] Carmen Ortiz Mellet,[e] Alberto Avenoza,[a] Jesús H. Busto,[a] Gonçalo J. L. Bernardes,[dh] Ramón Hurtado-Guerrero,[cij] Jesús M. Peregrina *[a] and Francisco Corzana *[a]

The Tn antigen (GalNAc-α-1-*O*-Thr/Ser) is a well-known tumor-associated carbohydrate determinant. The use of glycopeptides that incorporate this structure has become a significant and promising niche of research owing to their potential use as anticancer vaccines. Herein, the conformational preferences of a glycopeptide with an unnatural Tn antigen, characterized by a threonine decorated with an sp^2-iminosugar-type α-GalNAc mimic, have been studied both in solution, by combining NMR spectroscopy and molecular dynamics simulations, and in the solid state bound to an anti-mucin-1 (MUC1) antibody, by X-ray crystallography. The Tn surrogate can mimic the main conformer sampled by the natural antigen in solution and exhibits high affinity towards anti-MUC1 antibodies. Encouraged by these data, a cancer vaccine candidate based on this unnatural glycopeptide and conjugated to the carrier protein Keyhole Limpet Hemocyanin (KLH) has been prepared and tested in mice. Significantly, the experiments *in vivo* have proved that this vaccine elicits higher levels of specific anti-MUC1 IgG antibodies than the analog that bears the natural Tn antigen and that the elicited antibodies recognize human breast cancer cells with high selectivity. Altogether, we compile evidence to confirm that the presentation of the antigen, both in solution and in the bound state, plays a critical role in the efficacy of the designed cancer vaccines. Moreover, the outcomes derived from this vaccine prove that there is room for exploring further adjustments at the carbohydrate level that could contribute to designing more efficient cancer vaccines.

Received 15th December 2019
Accepted 26th March 2020

DOI: 10.1039/c9sc06334j

rsc.li/chemical-science

Introduction

The Tn antigen is a specific human tumor-associated carbohydrate antigen (TACA) formed by *N*-acetylgalactosamine (GalNAc) α-*O*-linked to either serine (Ser) or threonine (Thr) residues.[1] The overexpression of this simple structure correlates well with several types of tumors and it has been associated with metastatic behavior and tumor expansion. In general, the Tn antigen appears on the surface of epithelial cells as part of tumor-associated mucins. Mucins are heavily glycosylated proteins

[a]*Departamento de Química, Universidad de La Rioja, Centro de Investigación en Síntesis Química, E-26006 Logroño, Spain. E-mail: francisco.corzana@unirioja.es; jesusmanuel.peregrina@unirioja.es*

[b]*CIC BioGUNE, Bizkaia Technology, Park Building 800, 48170 Derio, Spain*

[c]*Institute of Biocomputation and Physics of Complex Systems (BIFI), University of Zaragoza, Zaragoza, Spain*

[d]*Instituto de Medicina Molecular, Faculdade de Medicina, Universidade de Lisboa, Avenida Professor Egas Moniz, 1649-028 Lisboa, Portugal*

[e]*Departamento de Química Orgánica, Facultad de Química, Universidad de Sevilla, E-41012 Sevilla, Spain*

[f]*Graduate School and Faculty of Advanced Life Science, Laboratory of Advanced Chemical Biology, Hokkaido University, N21 W11, Sapporo 001-0021, Japan*

[g]*Instituto de Investigaciones Químicas (IIQ), CSIC–Universidad de Sevilla, E-41092 Sevilla, Spain*

[h]*Department of Chemistry, University of Cambridge, Lensfield Road, CB2 1EW Cambridge, UK*

[i]*Copenhagen Center for Glycomics, Department of Cellular and Molecular Medicine, School of Dentistry, University of Copenhagen, Copenhagen, Denmark*

[j]*Fundación ARAID, Zaragoza, Spain*

† Electronic supplementary information (ESI) available. See DOI: 10.1039/c9sc06334j

that play a key role in several biological processes,[2] such as tissue inflammation, immune response or intercellular recognition. One of the most relevant mucins is MUC1,[3,4] which is composed of 20–125 tandem-type repeats of a core sequence of 20 amino acids "HGV**TS**APD**T**RPAPG**ST**APPA". This sequence presents five potential *O*-glycosylation sites made up of two Ser and three Thr residues (shown in bold letters in the tandem repeat sequence). In general, although this glycoprotein is decorated with complex *O*-glycans in healthy cells, in tumor tissues it usually presents simple carbohydrates, due mainly to the malfunction or relocation of GalNAc-transferases or mutations in COSMC, which is a chaperone for the follow-up glycosyltransferase C1GalT.[1,3,4] Consequently, different antigens that are masked in healthy cells, such as the Tn antigen, are exposed in malignancies and can trigger an immune response. Several studies have demonstrated the occurrence of anti-MUC1 antibodies in cancer patients that can limit tumor outgrowth and dissemination.[5–7] Moreover, the sequence PDTRP of MUC1 is the most immunogenic epitope recognized by anti-MUC1 antibodies,[8–10] such as the SM3 antibody, which has great potential to be used in early diagnosis and treatment of breast cancer.[11] For these reasons, MUC1 is considered a promising target for the development of cancer vaccines.[12–14] To date, most of these vaccines have failed in clinical trials.[3] An important drawback of these potential vaccines is their tendency to suffer from immunotolerance due to the presence of TACAs at low concentrations in healthy cells.[15] Additionally, the short biological half-life that some of these *O*-glycopeptides present is related to enzymatic degradation.[15,16] Thus, the use of unnatural TACA analogs that are more resistant to degradation and able to provide stronger and longer lasting immunogenicity represents an attractive and required niche of research in the development of anti-cancer vaccines.[17] Given that the *O*-glycosidic bond is particularly sensitive to enzymatic degradation in biological media, the incorporation of GalNAc moieties chemically modified in the anomeric region into carbohydrate-based cancer vaccines has attracted much attention in recent years.[18–22] These modifications included the use of C- and S-glycosides[23–25] or deoxyfluoroglycosides,[26–31] among others. We have recently contributed to this field by reporting the first examples of Tn antigens that feature a serine or a threonine glycosylated with a bicyclic sp^2-iminosugar moiety with a substitution and configurational pattern of structural complementarity to α-GalNAc (α-sp^2GalNAc),[32] namely compound **1a** and the corresponding mucin-related glycopeptide **2a** (Fig. 1). The presence of the sp^2-hybridized pseudoamide nitrogen at the position of the endocyclic oxygen in monosaccharides drastically enhances the anomeric effect in sp^2-iminosugar glycomimetics, which enables access to chemically and enzymatically stable α-linked conjugates with total stereocontrol.[33–35] We have also proved that the antibody scFv-SM3 exhibits a 2-fold higher affinity towards unnatural glycopeptide **2a** ($K_D = 1.60 \pm 0.16$ μM) relative to the natural variant **2b** ($K_D = 3.30 \pm 0.84$ μM).[32]

Here, we go one step further and report the synthesis and evaluation *in vivo* of a two-component anti-cancer vaccine (derivative **3a**), composed of Tn mimic α-sp^2 GalNAc-Thr (**1a**) in

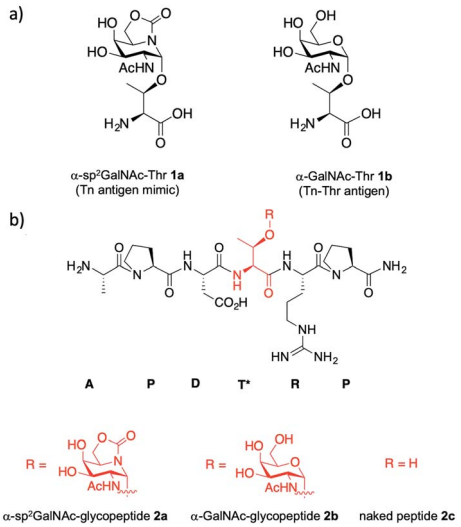

Fig. 1 (a) Structures of α-sp^2GalNAc-Thr **1a** and Tn antigen with threonine **1b**. (b) Structures of unnatural α-sp^2GalNAc-glycopeptide **2a** and the natural variants **2b** and **2c**.

the most immunogenic domain of a MUC1 fragment and immunogenic carrier protein Keyhole Limpet Hemocyanin[36] (KLH, Fig. 2). This protein was selected because it is one of the most popular protein carriers for carbohydrate-based cancer vaccines. Conjugates of this protein with several TACAs, such as Tn, GM2, GD2, Globo-H, and MUC1, have been used in clinical trials.[37–42] Moreover, it has been observed that KLH-MUC1 conjugates can elicit anti-MUC1 antibodies in human patients.[37,43–45] Conjugate **3b**, which displays natural Tn-Thr antigen GalNAc-α-1-*O*-Thr in its structure, was also synthesized and tested for comparison. In addition, and with the aim of providing a rational explanation for the higher binding affinity of the unnatural derivative, glycopeptide **2a** was synthesized and its structure was studied both in solution, through a combination of NMR spectroscopic experiments and molecular dynamics (MD) calculations, and in the solid state, by X-ray crystallography.

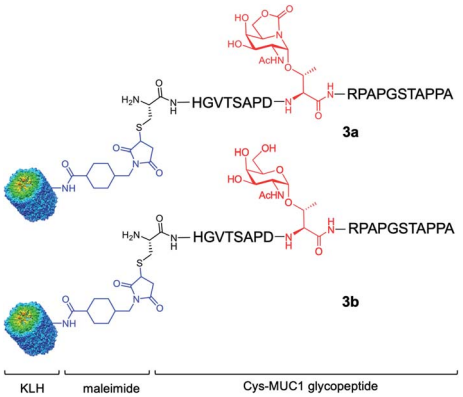

Fig. 2 Two-component cancer vaccine candidates **KLH-3a** (upper panel) and **KLH-3b** (lower panel) synthesized in this work from glycopeptides **3a** and **3b**, respectively.

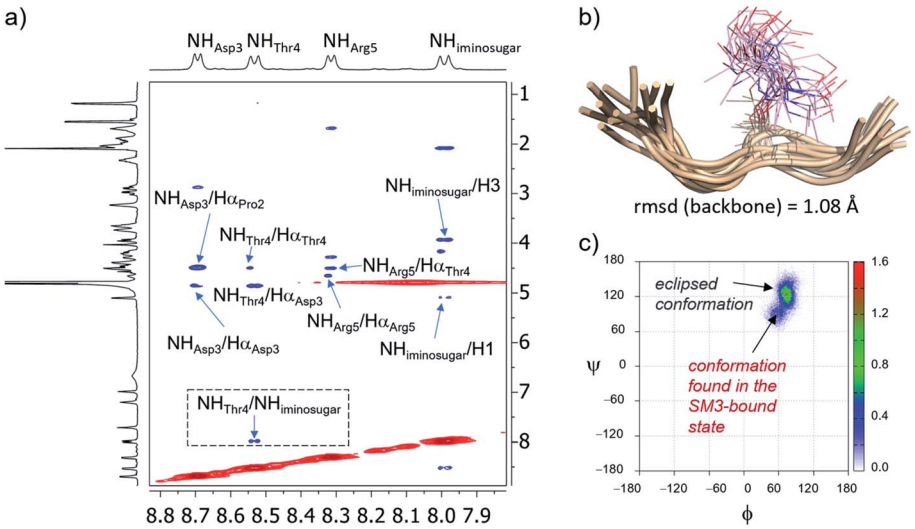

Fig. 3 (a) Section of the 2D NOESY spectrum (400 MHz) of glycopeptide **2a** in H_2O/D_2O (9 : 1) at 298 K, showing the amide region. Diagonal peaks and exchange cross-peaks connecting NH protons and water are negative (red). NOE contacts are represented as positive cross-peaks (blue). (b) Ensembles obtained from 20 ns experiment-guided MD simulations in explicit water for glycopeptide **2a**. Glycopeptide carbon atoms are shown in tan and the sugar moiety is in plum. (c) Distribution for the glycosidic linkage (ϕ/ψ) of **2a** derived from the 20 ns experiment-guided MD simulations.

Results and discussion

Unnatural glycopeptide **2a** presents a relatively high affinity towards the SM3 antibody. To verify this as a general trend, we analysed the binding of this derivative, as well as compounds **2b** and **2c**, with commercially available monoclonal antibody VU-11E2[2],[9,10] by using a microarray assay (Fig. S1 and S2†). The results derived from these experiments indicated that the antibody VU-11E2 has a preference for the glycosylated derivatives **2a** and **2b** relative to the naked peptide **2c**, which is in good agreement with previous studies.[9] However, in contrast to the SM3 antibody,[32] a slightly higher affinity of the

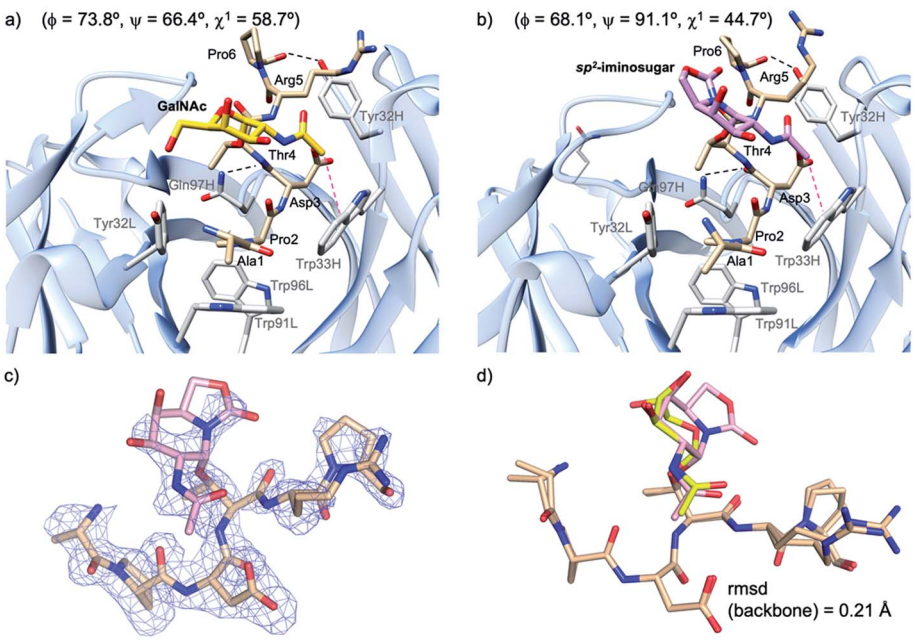

Fig. 4 Key binding interactions of glycopeptide **2b** (a) and **2a** (b) with antibody scFv-SM3, as observed in the X-ray crystal structure (pdb id: 5A2K and 6TGG, respectively). Pink dashed lines indicate the hydrophobic interaction between the sugar and the scFv-SM3 surface and black dashed lines indicate hydrogen bonds. The geometry of the glycosidic linkage is shown in parentheses. (c) Electron density maps are F_O-F_C syntheses (blue) contoured at 2.0σ for glycopeptide **2a**. (d) Superposition of the peptide backbone of glycopeptides **2a** and **2b** in complex with scFv-SM3. Peptide backbone carbon atoms are shown in tan. The sugar moiety in **2a** and **2b** is in plum and yellow, respectively.

VU-11E2 antibody was observed for natural glycopeptide **2b**. Therefore, the binding studies accomplished with SM3 and VU-11E2 antibodies showed that they recognize the unnatural glycopeptide **2a** and the natural variant **2b** with a comparable affinity, exhibiting a worse binding to the naked derivative **2c**.

To provide a rational explanation of the relatively high affinity of **2a** towards these anti-MUC1 antibodies, we performed the conformational analysis of this glycopeptide in solution and in the SM3-bound state.

In solution, 2D NOESY experiments showed key sequentially strong NH/Hα (i, i + 1) connectivities, such as $NH_{Asp}/H\alpha_{Pro}$, $NH_{Arg}/H\alpha_{Thr}$ or $NH_{Thr}/H\alpha_{Asp}$, along with weak or absent NH–NH (i, i + 1) NOE interactions, which suggests a preference for extended conformations of the peptide in solution[46] (Fig. 3a and Table S1†). These proton–proton distances were then used as

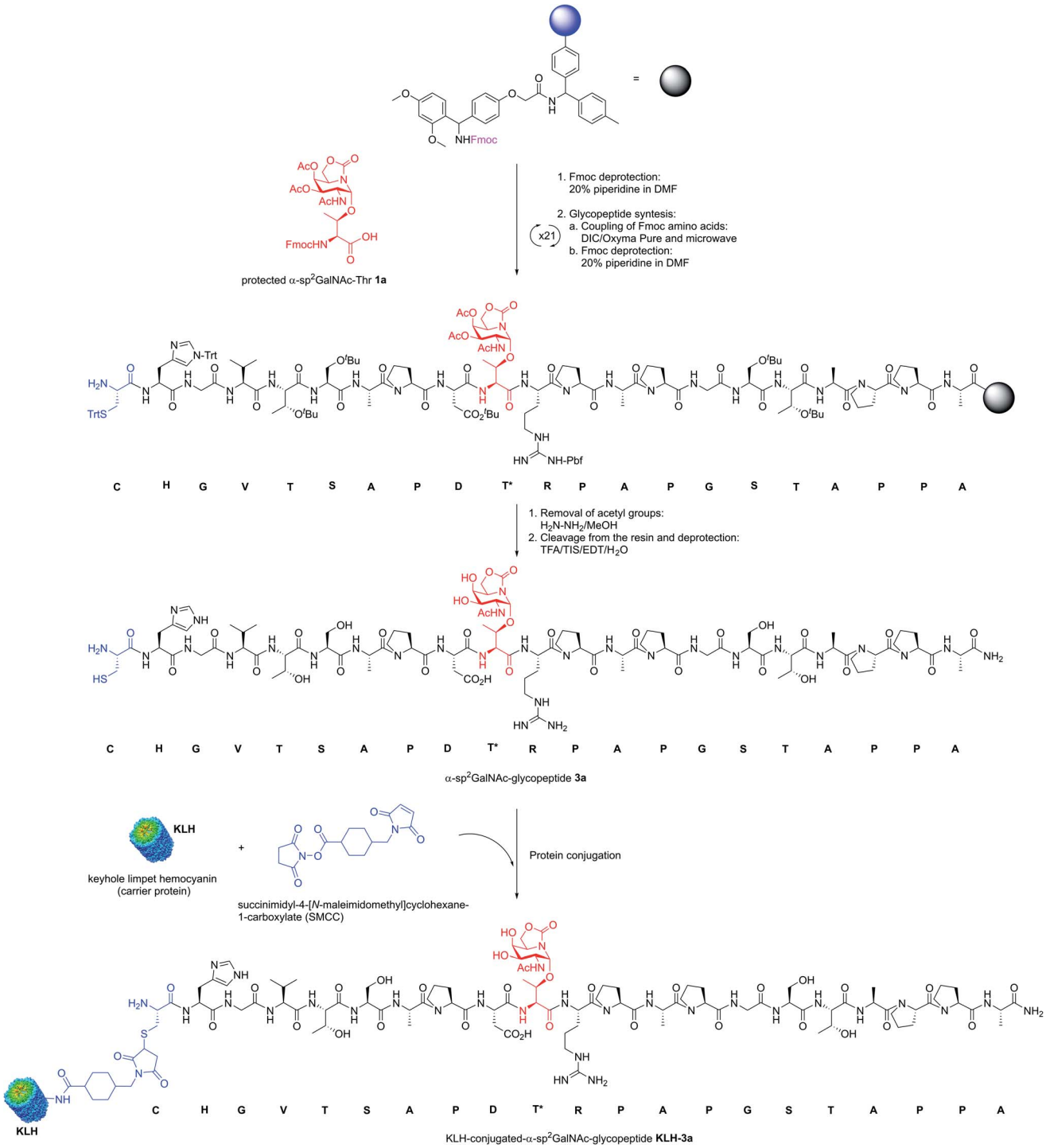

Scheme 1 Synthesis of KLH-conjugated-α-sp^{2}GalNAc-glycopeptide **KLH-3a** as a two-component cancer vaccine candidate.

restraints in experiment-guided MD simulations (MD simulations with time-averaged restraints; MD-tar),[47] following our well-established protocol.[48] These calculations were performed with AMBER 18 software,[49] implemented with ff14SB,[50] GLYCAM 06 (ref. 51) and general Amber force field (GAFF)[52] forcefields, and provided a distribution of low-energy conformers able to reproduce NOESY data. The good agreement between the experimental and calculated distances validates the theoretical study (Table S1†). Fig. 3b shows the structural ensemble derived from 20 ns experiment-guided MD simulations. According to these calculations, and in agreement with the NOE contacts, the peptide backbone of unnatural glycopeptide **2a** adopts an extended conformation in water (see also Fig. S3†). Moreover, the side-chain of the threonine derivative is quite rigid (χ^1 close to 60°), in agreement with previous studies.[53,54] Therefore, the conformational space sampled by the peptide fragment of compound **2a** is similar to that reported for the natural variant **2b**.[55]

Concerning the glycosidic linkage, the torsional angle ψ takes values of around 120°, which is characteristic of an eclipsed conformation (Fig. 3c).[53,54] This geometry is supported by a medium-size NOE cross-peak between the NH group of the threonine (NH_{Thr4}) residue and the NH of the sugar ($NH_{iminosugar}$, Fig. 3a). Of note, a low-populated conformer of the glycosidic linkage (population < 10%), characterized by values of ψ in the range of 60–90°, is also observed in solution. Markedly, this geometry of the glycosidic linkage, which is not populated by the natural variant **2b**,[55] is recognized by the SM3 antibody (see below).

Next, to evaluate compound **2a** in the bound state, we prepared high-quality crystals of the antibody scFv-SM3 in complex with this antigen and performed the subsequent crystallographic analysis. The structure, obtained at a resolution of 2.11 Å (Table S2†), reveals that the surface groove of the antibody nicely fits all the peptide residues (Fig. 4a), as previously observed for the natural glycopeptide **2b** and its naked variant (compound **2c** in Fig. 1).[55] Moreover, the conformation of the peptide backbone is almost identical to that displayed by **2b**, indicating that the presence of the unnatural sp^2-iminosugar within the GalNAc moiety does not significantly modify the overall conformation of the glycopeptide in the bound state (Fig. 4c).

The non-covalent interactions between the antibody and the unnatural antigen are the same as for **2b** and **2c**, involving several hydrogen bonds, some of them water-mediated, and stacking interactions. Thus, Pro2 stacks with Tyr32L, Trp91L and Trp96L, while Asp3 and Arg5 interact hydrophobically with Trp33H and Tyr32H, respectively. In addition, the CO group of Thr4 and Pro6 interacts through a hydrogen bond with Gln97H and Tyr32H, respectively.

The torsional angle ϕ of the glycosidic linkage takes a value close to 73°, in accordance with the exo-anomeric effect,[56] while ψ is close to 66°. This value of ψ, which is also exhibited by glycopeptide **2a** in the free state in solution, has not been detected for natural glycopeptide **2b** in the SM3-bound state. This characteristic geometry of the glycosidic linkage can enhance the CH/π interaction between the methyl group of the sugar and Trp33H (Fig. 4b).

It can be concluded that glycopeptide **2a** is quite rigid in solution and displays mainly a similar conformation to the natural variant **2b**. In the SM3-bound state, these two glycopeptides adopt a different disposition of the sugar moiety. Of note, in derivative **2a**, the *N*-acetyl group of the sugar is closer to a tryptophan residue, which is partly responsible for the better binding of the unnatural glycopeptide. This, together with the occurrence of this conformer in solution, may explain the better affinity reported for unnatural glycopeptide **2a** relative to the natural derivative **2b**.

Encouraged by the high capacity of derivative **2a** to mimic the natural antigen, we carried out the synthesis of two-component cancer vaccine[57] **KLH-3a** (Fig. 2), together with the natural variant **KLH-3b** for comparison. Vaccine **KLH-3a** combines MUC1-glycopeptide **3a** (Scheme 1), which features sp^2-iminosugar Tn mimic **1a** in the tandem repeat sequence of MUC1 and a Cys residue at its *N*-terminus to allow the conjugation to the immunogenic carrier protein KLH. The synthesis of **3a** was accomplished by using microwave-assisted solid phase peptide synthesis (MW-SPPS). Once purified by reverse-phase (RP)-HPLC and lyophilized, compound **3a** was conjugated to the KLH protein by the maleimide protocol by using succinimidyl-4-(*N*-maleimidomethyl)cyclohexane-1-carboxylate (SMCC) as a heterobifunctional linker (Scheme 1). Natural MUC1 derivative **3b** and naked peptide **3c** (see the ESI†), which contain antigen **1b** or a threonine residue, respectively, were prepared following the same protocol as described in Scheme 1. The yield of the conjugation reactions of derivatives **3a** and **3b** to KLH was estimated by immunoassay experiments[58] and determined by UPLC/MS (see Experimental section).

Next, Balb/c mice were immunized with **KLH-3a** and **KLH-3b** four times at biweekly intervals. The first immunizations were performed with complete Freund's adjuvant and the others were accomplished with incomplete Freund's adjuvant. One week after the last immunization, the mice were sacrificed, and serum was harvested. Murine IgG and IgM antibody responses of sera were characterized by ELISA. As can be seen in Fig. 5 and S4,† mice immunized with these vaccine candidates elicited a specific anti-MUC1 IgG antibody response and, more importantly, the unnatural vaccine **KLH-3a** was able to elicit higher levels of IgG antibodies in comparison to the natural variant

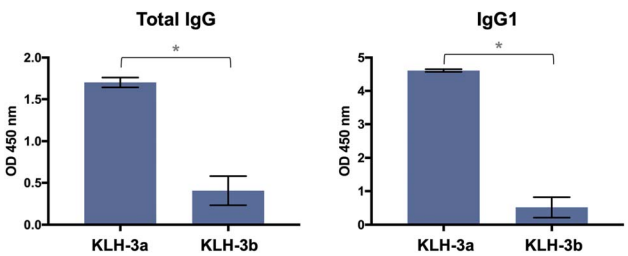

Fig. 5 Total IgG and sub-typing (IgG1) anti-MUC1 antibody titrations after immunization with either vaccine **KLH-3a** or **KLH-3b**. ELISA plates were coated with natural MUC1-like glycopeptide **3b**. The horizontal lines indicate the mean for the group of mice ($n = 3$). An asterisk indicates a statistically significant difference (*$P < 0.05$).

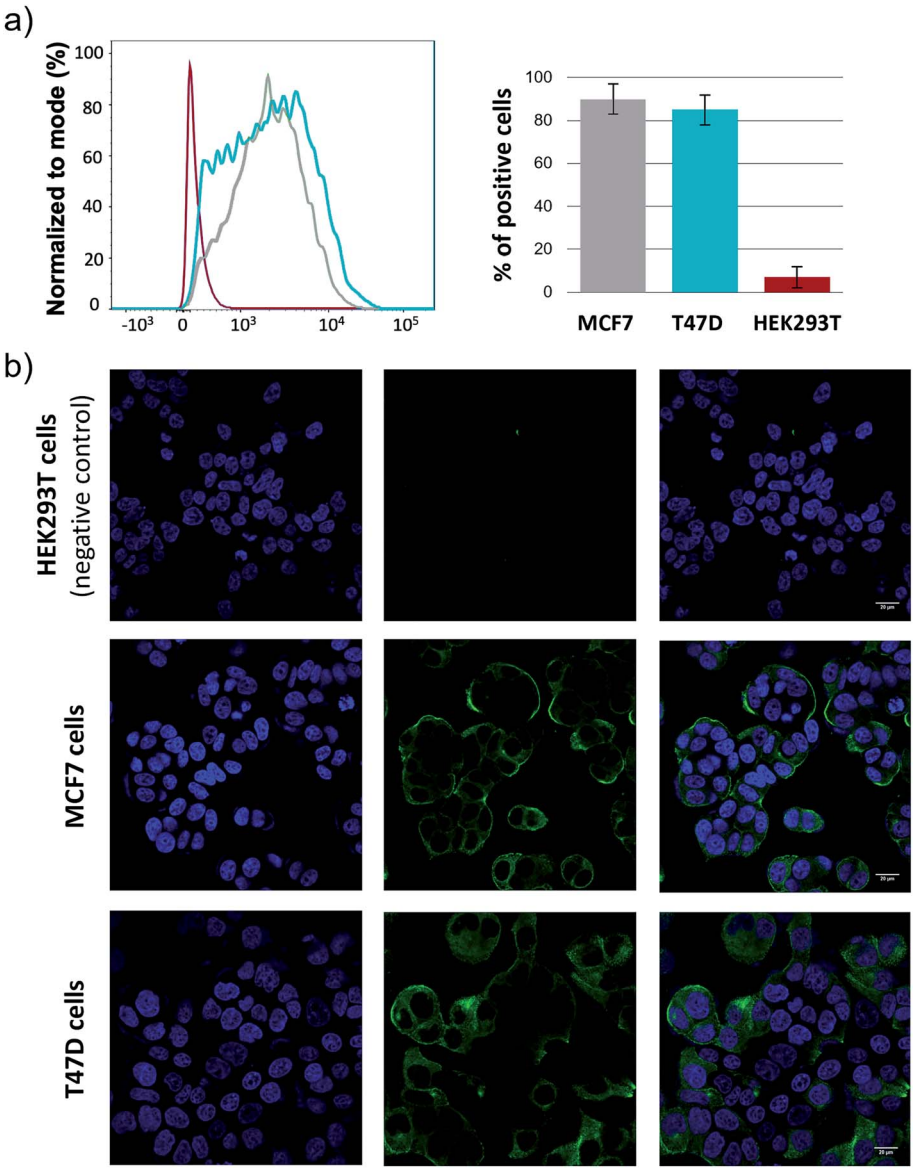

Fig. 6 a) Staining of living cells with the antisera of mice immunized with **KLH-3a** analyzed by flow cytometry: HEK293T (red line), T47D (blue line) and MCF7 (grey line). Staining with a 1 : 100 dilution of sera and visualization with a mouse secondary α-IgG-488 antibody. (b) Confocal microscopy images show that mice antisera after vaccination with **KLH-3a** stain breast cancer cells MCF7 and T47D expressing tumor-associated MUC1, but not those that do not express tumor-associated MUC1 on their surface, HEK293T. Blue = Hoechst (nuclei); green = secondary anti-mouse IgG Alexa 488 (tumor-associated MUC1).

KLH-3b. Regarding sub-typing of the IgG antibodies, both vaccines show IgG1 titers significantly higher than IgG2a (Fig. 5 and S4†), which indicates a prevalence of a Th1 response (humoral immunity).[59,60] The data also reveal that a T cell-mediated class-switching takes place, because IgM antibody values were low with both vaccines (Fig. S4†).[14] However, antibodies produced by both vaccines recognized likewise glycosylated and naked MUC1 epitopes (Fig. S5†). This result indicates that the elicited antibodies target mainly the peptide and not the glycan moiety.

Finally, it is important to note that the elicited antibodies can selectively recognize native tumor associated MUC1 presented on the surface of human cancer cells. To demonstrate this, MCF7 and T47D cell lines, which express tumor associated MUC1 on their surface, together with a human embryonic kidney cell line (HEK293T), which was used as a negative control, were treated with antisera obtained after immunization with **KLH-3a** and analyzed by flow cytometry.[48] The experiments showed that MCF7 and T47D strongly react with the antisera, while HEK293T cells were not targeted (Fig. 6a). These results support subsequent confocal microscopy experiments (Fig. 6b). Taken together, this result suggests that antibodies generated after the immunization of mice with unnatural vaccine **KLH-3a** can selectively recognize human cancer cells.

Conclusions

A MUC1-like glycopeptide with an unnatural Tn antigen that features a threonine glycosylated with an sp^2-iminosugar GalNAc mimetic has been conjugated to the carrier protein KLH and tested in mice. The experiments *in vivo* show that this vaccine elicits specific anti-MUC1 IgG antibodies that outnumber those obtained with the natural analog. More importantly, these antibodies are able to recognize human cancer cell lines that express tumor associated MUC1 on their surface. On the one hand, the absence of the sp^2-iminosugars in organisms might enhance the immunogenicity of the designed antigen. This feature, combined with the resistance of this unnatural scaffold to degradation, could contribute significantly to the effectiveness of the vaccine. On the other hand, the conformational analysis performed by NMR spectroscopy and MD simulations demonstrates that the unnatural derivative is rigid in solution and adopts a geometry similar to that found for the natural Tn-glycopeptide. According to the crystallographic analysis, the SM3-bound state reveals that the glycosidic linkage of the unnatural glycopeptide displays an orientation that facilitates the CH/π interaction between the methyl of the *N*-acetyl group of the sugar and a tryptophan residue, which is partly responsible for the better binding of the unnatural glycopeptide. As we have previously reported, rather flexible determinants can hinder the boosting of the immune system.[61] Thus, according to the present work, when the engineered antigen is capable of copying the conformational landscape of the natural Tn antigen and exhibits a good affinity towards anti-MUC1 antibodies, this determinant is *a priori* a good candidate to develop effective cancer vaccines.[48]

Therefore, the results reported in this work can contribute to exploiting the rational design of cancer vaccines.

Experimental section

Reagents and general procedures

Commercial reagents were used without further purification. Solvents were dried and redistilled prior to use in the usual way. ^{1}H and ^{13}C NMR spectra were measured with Bruker Avance-400 and Bruker ARX-300 spectrometers in D_2O or H_2O/D_2O (9 : 1) at 298 K. Spectra were assigned by using COSY and HSQC. High-resolution electrospray ionization (ESI) mass spectra were recorded on a microTOF-Q-BRUKER spectrometer; accurate mass measurements were achieved by using sodium formate as an external reference.

NMR experiments

NMR experiments were performed with a 400 MHz spectrometer at 298 K. Magnitude-mode ge-2D COSY spectra were acquired with gradients by using the *cosygpqf* pulse program with a pulse width of 90°. Phase-sensitive ge-2D HSQC spectra were acquired by using a z-filter and selection before t1, removing the decoupling during acquisition by use of the *invigpndph* pulse program with CNST2 (JHC) = 145.

2D NOESY experiments

NOESY experiments were performed with a Bruker Avance 400 MHz spectrometer at 298 K and pH 6.0–6.5 in H_2O/D_2O (9 : 1). The experiments were conducted by using phase-sensitive ge-2D NOESY with WATERGATE for H_2O/D_2O (9 : 1) spectra. NOE intensities were normalized with respect to the diagonal peak at zero mixing time. Distances involving NH protons were semi-quantitatively determined by integrating the volume of the corresponding cross-peaks. The number of scans used was 16 and the mixing time was 500 ms.

Microwave assisted solid-phase peptide synthesis (MW-SPPS)

This synthesis was performed automatically with Rink Amide MBHA resin (0.05 mmol) and an automated synthesizer. DIC/Oxyma Pure® was used as the coupling reagent and 20% (v/v) solution of piperidine in dimethylformamide (DMF) was used for fluorenylmethyloxycarbonyl (Fmoc) deprotection. The glycosylated amino acid building blocks were synthesized as described in the literature:[32,62] the corresponding amino acid (1.5 equiv.) together with 2-(1*H*-benzotriazol-1-yl)-1,1,3,3-tetramethyluronium hexafluorophosphate (HBTU; 0.9 equiv.) and 0.25 mL of *N*,*N*-diisopropylethylamine [DIPEA; 2.0 M in *N*-methyl-2-pyrrolidone (NMP)] were dissolved in 2 mL of DMF. The reaction mixture was added to the resin and vortex mixed for 3 h, until the coupling was completed as deduced by the Kaiser test. *O*-Acetyl groups of the carbohydrates were deprotected with 5 mL (3 × 15 min) of a hydrazine/MeOH (7 : 3) solution. (Glyco)peptides were detached from the resin and acid-sensitive sidechain protecting groups by treatment with a solution of trifluoroacetic acid (TFA)/triisopropylsilane (TIS)/H_2O/1,2-ethanedithiol (EDT; 92.5 : 2.5 : 2.5 : 2.5) for 3 h at 25 °C. (Glyco)peptides were then precipitated with cold diethyl ether and centrifuged, to afford the crude derivatives. Purification by RP-HPLC afforded the corresponding (glyco)peptides (for experimental details see the ESI†).

Microarrays

Anti-MUC1 mouse monoclonal antibody VU-11E2 (0.86 mg mL^{-1}) and FluoroLinkTM CyTM3-labeled goat anti-mouse IgG were used in these experiments. The *microarray printing* and the microarray monoclonal antibody binding assay were performed following the same protocols previously reported by us[63] (for experimental details see the ESI and Fig. S1 and S2†).

Molecular dynamics simulations with time averaged restraints (MD-tar)

The simulations were carried out with the AMBER 18 package,[49] and implemented with ff14SB (ref. 50) and GAFF.[52] Parameters for the unnatural sugar mimic were generated with the antechamber module of AMBER 18, with partial charges set to fit the electrostatic potential generated with HF/6-31G(d) by RESP.[64] The charges were calculated according to the Merz–Singh–Kollman scheme with Gaussian 16.[65] The system was neutralized by adding explicit counter ions (Cl^-). Prior to MD-tar[47] productive simulation on glycopeptide **2a**, we performed an

equilibration protocol consisting of an initial minimization of the water box of 5000 steps, followed by a 2500-step minimization of the whole system. Then, the TIP3P[66] water box was heated at constant volume until 298 K by using a time constant for a heat bath coupling of 1 ps. The equilibration finished with 200 ps of MD simulation without restraints, at a constant pressure of 1 bar and temperature of 298 K, turning on the Langevin temperature scaling with a collision frequency of 1 ps. An 8 Å cutoff was applied to Lennard-Jones interactions. Periodic boundary conditions and the particle mesh Ewald method[67] were turned on in every step of the equilibration protocol to evaluate the long-range electrostatic forces, using a grid spacing of 1 Å. 20 ns MD-tar[47] simulations were run with the same settings used in the last step of the equilibration protocol. A time step of 1 fs was used. The NOE-derived distances shown in Table S1† were imposed as time-averaged restraints, applying an r^{-6} averaging. The equilibrium distance range was set to $r_{exp} - 0.2$ Å $\leq r_{exp} \leq r_{exp} + 0.2$ Å. The force constants r_{k_2} and r_{k_3} used in each case were 10 kcal mol^{-1}·Å^{-2}. A decay constant of 2000 ps was used throughout the MD simulations. The coordinates were saved each 1 ps, thus obtaining MD trajectories of 20 000 frames. The analysis of the MD-tar trajectories has been carried out with the *cpptraj* module of AMBER 18.

Crystallization

Expression and purification of scFv-SM3 has been described previously by us.[55] Crystals were grown by sitting drop diffusion at 18 °C. The drops were prepared by mixing 0.5 μL of protein solution, which contained 15 mg mL^{-1} scFv-SM3 and 10 mM glycopeptide **2a** with 0.5 μL of the mother liquor. Crystals of scFv-SM3 with the peptide above were grown in 20% PEG 3350 in 0.2 M disodium hydrogen phosphate. The crystals were cryoprotected in mother liquor containing 15% ethylene glycol and frozen in a nitrogen gas stream cooled to 100 K.

Structure determination and refinement

Diffraction data were collected on synchrotron beamline I24 of the Diamond Light Source (Harwell Science and Innovation Campus, Oxfordshire, UK) at a wavelength of 0.97 Å and a temperature of 100 K. Data were processed and scaled with the XDS package[68] and CCP4 software.[69,70] Relevant statistics are given in Table S2.† The crystal structures were solved by molecular replacement with Phaser[69,70] and by using the PDB entry 1SM3 as the template. Initial phases were further improved by cycles of manual model building in Coot[71] and refinement with REFMAC5.[72] The final models were validated with PROCHECK.[73] Coordinates and structure factors have been deposited in the Worldwide Protein Data Bank (wwPDB; PDB id 6TGG).

Conjugation

Conjugation of MUC1 derivatives was conducted by INYCOM Biotech (Zaragoza, Spain) following a standard procedure as follows. First, SMCC (2 mg) was dissolved in 10 μL of DMF and then added to a KLH solution (50 μL, 20 mg mL^{-1} in phosphate-buffered saline (PBS), pH 7.2). The mixture was diluted by adding 25 μL of PBS. After 1 h at room temperature, the mixture was diluted with 175 μL of PBS and purified by using dialysis (14 kDa MWCO) against PBS for 24 h. Glycopeptides (2 mg dissolved in 500 μL of PBS) were treated with KLH-SMCC (2 mg in 200 μL of PBS). After 2 h at room temperature, the mixture was purified by using dialysis (14 kDa MWCO) against PBS for 24 h. The total protein concentration (absorbance at 280 nm) was 1.1 and 1.0 mg mL^{-1} for **KLH-3a** and **KLH-3b**, respectively. The glycopeptide/KLH ratio was determined by UPLC/MS,[74] using glycopeptides **3a** and **3b** as standards (Fig. S6†). The experimentally calculated values were **3a**/KLH = 3305 and **3b**/KLH = 3420.

Immunizations

Immunizations were carried out by INYCOM Biotech (Zaragoza, Spain). Three female MUC1.Tg mice (Balb/c) that express human MUC1 at the physiological level (14-week-old, average weight = 24 g) were immunized four times at biweekly intervals at the base of the tail intradermally with vaccine **KLH-3a** or **KLH-3b** (25 μg), together with complete or incomplete Freund's adjuvant. The endpoint was one week after the 4th immunization.

Serologic assays

Anti-MUC1 IgG, IgG1, IgG2a, IgG2b, IgG3 and IgM antibody titers were determined by enzyme-linked immunosorbent assay, which was conducted by INYCOM Biotech (Zaragoza, Spain) as follows. ELISA plates (JetBioFil, China) were coated with 75 μL of a 5 μg mL^{-1} solution of either **3b** or **3c** in PBS and incubated for 1 h at 37 °C. Unreacted sites were blocked with 225 μL of BSA 1% in washing buffer (0.05% Tween-20 in PBS 1×) for 1 h at 37 °C. Afterwards, wells were washed twice with washing buffer. 75 μL of serum samples (blood taken from each mouse's tail diluted in 800 μL of BSA 1% solution) were allowed to bind to immobilized antigens for 30 min at 37 °C. Wells were then washed twice with washing buffer, prior to incubation with 75 μL of biotinylated anti-mouse antibodies (1 : 1000 dilution in conjugated solvent) for 30 min at 37 °C. After washing three times with washing buffer, incubation with 75 μL streptavidin-HRP (Sigma), 1 : 500 dilution in conjugation solvent, was carried out for 30 min at 37 °C. Wells were washed five times with washing buffer. 75 μL of TMB were then incubated for 5 min at room temperature. For the final color-developing step, 75 μL of 0.2 M HCl were added to stop the reaction. Absorbance at 450 nm was read, using an iMark™ BIO RAD Microplate Reader. Comparisons were performed by using an unpaired *t* test with equal SD. Differences were considered significant when $P < 0.05$.

Culture of cell lines

Three different cell lines were used for the *in vitro* studies, namely HEK293T (a human embryonic kidney cell line), MCF7 (a human breast adenocarcinoma cell line) and T47D cells (a human breast ductal carcinoma cell line). The cells were maintained in a humidified incubator at 37 °C under 5% CO_2

and grown by using 1× DMEM (Dulbecco's modified Eagle's medium) with sodium pyruvate and without L-glutamine (Invitrogen, Life Technologies) supplemented with 10% heat-inactivated fetal bovine serum (FBS) (Gibco, Life Technologies), 1× MEM NEAA (Gibco, Life Technologies), 1× GlutaMAX (Gibco, Life Technologies), 200 units per mL penicillin and 200 μg mL^{-1} streptomycin (Gibco, Life Technologies) and 10 mM HEPES (Gibco, Life Technologies). The medium of the T47D cells was supplemented with 10 μg mL^{-1} insulin (Gibco, Life Technologies).

Reactivity of antibodies towards human cancer cell lines determined by flow cytometry analysis

The reactivity of the antibodies elicited by **KLH-3a** towards breast cancer cell lines was determined by staining the cells with the antisera followed by flow cytometry analysis. For this purpose, MCF7 and T47D cells (with high expression of TA-MUC1) and HEK293T cells (with no expression of TA-MUC1) were fixed with an ice-cold solution of 4% paraformaldehyde in PBS (100 000 cells per FACS tube) for 10 min. After fixation, the cells were subjected to a permeabilization step with 0.1% Triton-X100 in PBS for 15 min, followed by a blocking step with 10% FBS in PBS for 30 min. The cells were then incubated with 50 μL of 1 : 50 dilution of mice sera. After 1 h of incubation, cells were incubated with 50 μL per·well of goat anti-mouse polyclonal IgG H&L Alexa Fluor 488 (1 : 2000) secondary antibody from Abcam, for an additional 1 h. All the incubation periods were completed at rt and were followed by washing steps with PBS (with 4 min centrifugation at 4000 rpm to remove the supernatant). Acquisition was done with a BD LSR Fortessa setup with a 488 nm laser and a 530/30 nm band-pass filter (combination used for Alexa488 detection). Data analysis was done with FlowJo (version 6.3.4, FlowJo) software.

Reactivity of antibodies towards human breast cancer cell lines analyzed by confocal microscopy

Antiserum staining of cell lines MCF7, T47D and HEK293T (negative control) was investigated by confocal microscopy. To this end, 30 000 cells per well were seeded in 8-well μ-Slide Ibidi Plates and grown for 24 h. The cells were then incubated with CellMask Deep Red membrane dye (1 : 1000) for 10 min at 37 °C, followed by a fixation step with 4% paraformaldehyde in PBS for 10 min at 37 °C. The cells were then washed with PBS and permeabilized with 1% Triton X-100 in PBS for 15 min at rt. The cells were then incubated with the mice sera (1 : 100 dilution) at 4 °C overnight. The cells were washed with PBS and incubated with 200 μL per well of goat anti-mouse polyclonal IgG H&L Alexa Fluor 488 (1 : 2000) secondary antibody from Abcam, for 2 h at rt. Finally, the cells were washed and incubated with Hoechst (1 μg mL^{-1}) for 10 min at rt to stain the nuclei and analyzed with a Zeiss LSM 710 confocal laser point-scanning microscope with a 40× oil objective and numerical aperture = 1.3. The secondary antibody was visualized with an argon laser source (488 nm, emission 500–550 nm), while CellMask Deep Red stained membranes were visualized upon excitation with a DPSS 561-10 laser (561 nm, emission 570–640 nm), and nuclei were visualized with a diode 405-30 laser (450 nm, emission 420–470 nm).

Author contributions

I. A. B., C. D. N. and A. A. synthesized, purified and characterized the glycopeptides. J. H. B. and J. M. P. and F. C. performed and analyzed the NOESY experiments. J. C.-L. and R. H.-G. purified antibody scFv-SM3, crystallized the complex and refined the crystal structure. A. G. and G. J. L. B. carried out the flow cytometry and the confocal microscopy experiments. E. M. S. F, J. M. G. F. and C. O. M. performed the synthesis, purification and characterization of the unnatural building bock with the sp^2-iminosugar to use in solid-phase peptide synthesis. F. G.-M., H. H. and S.-I. N. carried out the microarray assays. I. A. B. and E. J.-M. determined the glycopeptide/KLH ratio by using UPLC/MS. F. C. performed the conformational analysis of the antigen in solution. F. C. and J. M. P. wrote the article with the other authors' contributions. All authors read and approved the final manuscript.

Conflicts of interest

There are no conflicts to declare.

Acknowledgements

We acknowledge the Ministerio de Ciencia, Innovación y Universidades and the Agencia Estatal de Investigación (projects RTI2018-099592-B-C21 and RTI2018-097609-B-C21), the Ministerio de Economía y Competitividad (SAF2016-76083-R), European Regional Development Funds (FEDER-UE), the Royal Society (URF\R\180019 to G. J. L. B.) and FCT Portugal (PhD studentship, SFRH/BD/115932/2016 to A. G. and FCT Investigator IF/00624/2015 to G. J. L. B.). M. C. O further thanks CITIUS for technical support. I. A. B. thanks the Asociación Española Contra el Cancer en La Rioja for a grant. E. J.-M. thanks Universidad de La Rioja for a postdoctoral fellowship. R. H.-G. acknowledges Diamond Light Source (Oxford, UK) synchrotron beamline I04 (experiment numbers mx10121-19). He also acknowledges ARAID, MEC (CTQ2013-44367-C2-2-P and BFU2016-75633-P) and Gobierno de Aragón (E34_R17 and LMP58_18) with FEDER (2014–2020) funds for 'Building Europe from Aragón' for financial support. The research leading to these results has also received funding from FP7 442 (2007–2013) under BioStruct-X (grant agreement no. 283570 and BIOSTRUCTX_5186). F. G.-M. of Hokkaido University acknowledges grant from the Naito Foundation. INYCOM Biotech (Zaragoza, Spain) has the required approval statements to perform studies with animals. The authors thank Dr Vikki Cantrill for her help with the editing of this manuscript.

References

1 T. Ju, V. I. Otto and R. D. Cummings, *Angew. Chem., Int. Ed.*, 2011, **50**, 1770–1791.
2 D. W. Kufe, *Nat. Rev. Cancer*, 2009, **9**, 874–885.

3 J. Taylor-Papadimitriou, J. M. Burchell, R. Graham and R. Beatson, *Biochem. Soc. Trans.*, 2018, **46**, 659–668.
4 V. Apostolopoulos, L. Stojanovska and S. E. Gargosky, *Cell. Mol. Life Sci.*, 2015, **72**, 4475–4500.
5 O. Blixt, D. Bueti, B. Burford, D. Allen, S. Julien, M. Hollingsworth, A. Gammerman, I. Fentiman, J. Taylor-Papadimitriou and J. M. Burchell, *Breast Cancer Res.*, 2011, **13**, R25.
6 H. Chen, S. Werner, S. Tao, I. Zörnig and H. Brenner, *Cancer Lett.*, 2014, **346**, 178–187.
7 Z. M. Tang, Z. G. Ling, C. M. Wang, Y. Bin Wu and J. L. Kong, *PLoS One*, 2017, **12**, e0182117.
8 H. Takeuchi, K. Kato, K. Denda-Nagai, F. G. Hanisch, H. Clausen and T. Irimura, *J. Immunol. Methods*, 2002, **270**, 199–209.
9 U. Karsten, N. Serttas, H. Paulsen, A. Danielczyk and S. Goletz, *Glycobiology*, 2004, **14**, 681–692.
10 Y. Yoshimura, K. Denda-Nagai, Y. Takahashi, I. Nagashima, H. Shimizu, T. Kishimoto, M. Noji, S. Shichino, Y. Chiba and T. Irimura, *Sci. Rep.*, 2019, **9**, 16641.
11 P. Dokurno, P. A. Bates, H. A. Band, L. M. D. Stewart, J. M. Lally, J. M. Burchell, J. Taylor-Papadimitriou, D. Snary, M. J. E. Sternberg and P. S. Freemont, *J. Mol. Biol.*, 1998, **284**, 713–728.
12 N. Gaidzik, U. Westerlind and H. Kunz, *Chem. Soc. Rev.*, 2013, **42**, 4421–4442.
13 M. A. Wolfert and G.-J. Boons, *Nat. Chem. Biol.*, 2013, **9**, 776.
14 R. M. Wilson and S. J. Danishefsky, *J. Am. Chem. Soc.*, 2013, **135**, 14462–14472.
15 G. L. Beatty and W. L. Gladney, *Clin. Cancer Res.*, 2015, **21**, 687–692.
16 C. Nativi, F. Papi and S. Roelens, *Chem. Commun.*, 2019, **55**, 7729–7736.
17 N. Martínez-Sáez, J. M. Peregrina and F. Corzana, *Chem. Soc. Rev.*, 2017, **46**, 7154–7175.
18 Z. Guo and Q. Wang, *Curr. Opin. Chem. Biol.*, 2009, **13**, 608–617.
19 Q. Wang, S. A. Ekanayaka, J. Wu, J. Zhang and Z. Guo, *Bioconjugate Chem.*, 2008, **19**, 2060–2067.
20 Q. Wang and Z. Guo, *ACS Med. Chem. Lett.*, 2011, **2**, 373–378.
21 C.-C. Liu and X.-S. Ye, *Glycoconjugate J.*, 2012, **29**, 259–271.
22 B. Richichi, B. Thomas, M. Fiore, R. Bosco, H. Qureshi, C. Nativi, O. Renaudet and L. BenMohamed, *Angew. Chem., Int. Ed.*, 2014, **53**, 11917–11920.
23 B. Kuberan, S. A. Sikkander, H. Tomiyama and R. J. Linhardt, *Angew. Chem., Int. Ed.*, 2003, **42**, 2073–2075.
24 L. Awad, R. Madani, A. Gillig, M. Kolympadi, M. Philgren, A. Muhs, C. Gérard and P. Vogel, *Chem.–Eur. J.*, 2012, **18**, 8578–8582.
25 D. R. Bundle, J. R. Rich, S. Jacques, H. N. Yu, M. Nitz and C.-C. Ling, *Angew. Chem., Int. Ed.*, 2005, **44**, 7725–7729.
26 C. Mersch, S. Wagner and A. Hoffmann-Röder, *Synlett*, 2009, 2167–2171.
27 M. Johannes, M. Reindl, B. Gerlitzki, E. Schmitt and A. Hoffmann-Röder, *Beilstein J. Org. Chem.*, 2015, **11**, 155–161.
28 A. Hoffmann-Röder, A. Kaiser, S. Wagner, N. Gaidzik, D. Kowalczyk, U. Westerlind, B. Gerlitzki, E. Schmitt and H. Kunz, *Angew. Chem., Int. Ed.*, 2010, **49**, 8498–8503.
29 F. Yang, X.-J. Zheng, C.-X. Huo, Y. Wang, Y. Zhang and X.-S. Ye, *ACS Chem. Biol.*, 2011, **6**, 252–259.
30 A. Hoffmann-Röder and M. Johannes, *Chem. Commun.*, 2011, **47**, 9903–9905.
31 T. Oberbillig, C. Mersch, S. Wagner and A. Hoffmann-Röder, *Chem. Commun.*, 2012, **48**, 1487–1489.
32 E. M. Sánchez Fernández, C. D. Navo, N. Martínez-Sáez, R. Gonçalves-Pereira, V. J. Somovilla, A. Avenoza, J. H. Busto, G. J. L. Bernardes, G. Jiménez-Osés, F. Corzana, J. M. García Fernández, C. Ortiz Mellet and J. M. Peregrina, *Org. Lett.*, 2016, **18**, 3890–3893.
33 E. M. Sánchez-Fernández, R. Rísquez-Cuadro, M. Chasseraud, A. Ahidouch, C. Ortiz Mellet, H. Ouadid-Ahidouch and J. M. García Fernández, *Chem. Commun.*, 2010, **46**, 5328–5330.
34 E. M. Sánchez-Fernández, R. Rísquez-Cuadro, C. Ortiz Mellet, J. M. García Fernández, P. M. Nieto and J. Angulo, *Chem.–Eur. J.*, 2012, **18**, 8527–8539.
35 R. Rísquez-Cuadro, R. Matsumoto, F. Ortega-Caballero, E. Nanba, K. Higaki, J. M. García Fernández and C. Ortiz Mellet, *J. Med. Chem.*, 2019, **62**, 5832–5843.
36 J. R. Harris and J. Markl, *Micron*, 1999, **30**, 597–623.
37 S. Adluri, T. Gilewski, S. Zhang, V. Ramnath, G. Ragupathi and P. Livingston, *Br. J. Cancer*, 1999, **79**, 1806–1812.
38 A. M. M. Eggermont, S. Suciu, P. Rutkowski, J. Marsden, M. Santinami, P. Corrie, S. Aamdal, P. A. Ascierto, P. M. Patel, W. H. Kruit, L. Bastholt, L. Borgognoni, M. G. Bernengo, N. Davidson, L. Polders, M. Praet and A. Spatz, *J. Clin. Oncol.*, 2013, **31**, 3831–3837.
39 D. Miles, H. Roché, M. Martin, T. J. Perren, D. A. Cameron, J. Glaspy, D. Dodwell, J. Parker, J. Mayordomo, A. Tres, J. L. Murray and N. K. Ibrahim, *Oncologist*, 2011, **16**, 1092–1100.
40 J. Zhu, Q. Wan, D. Lee, G. Yang, M. K. Spassova, O. Ouerfelli, G. Ragupathi, P. Damani, P. O. Livingston and S. J. Danishefsky, *J. Am. Chem. Soc.*, 2009, **131**, 9298–9303.
41 P. J. Sabbatini, V. Kudryashov, G. Ragupathi, S. J. Danishefsky, P. O. Livingston, W. Bornmann, M. Spassova, A. Zatorski, D. Spriggs, C. Aghajanian, S. Soignet, M. Peyton, C. O'Flaherty, J. Curtin and K. O. Lloyd, *Int. J. Cancer*, 2000, **87**, 79–85.
42 S. J. Danishefsky and J. R. Allen, *Angew. Chem., Int. Ed.*, 2000, **39**, 836–863.
43 T. Gilewski, S. Adluri, G. Ragupathi, S. Zhang, T.-J. Yao, K. Panageas, M. Moynahan, A. Houghton, L. Norton and P. O. Livingston, *Clin. Cancer Res.*, 2000, **6**, 1693–1701.
44 P. J. Sabbatini, G. Ragupathi, C. Hood, C. A. Aghajanian, M. Juretzka, A. Iasonos, M. L. Hensley, M. K. Spassova, O. Ouerfelli, D. R. Spriggs, W. P. Tew, J. Konner, H. Clausen, N. Abu Rustum, S. J. Dansihefsky and P. O. Livingston, *Clin. Cancer Res.*, 2007, **13**, 4170–4177.
45 C. Musselli, P. O. Livingston and G. Ragupathi, *J. Cancer Res. Clin. Oncol.*, 2001, **127**, R20–R26.

46 H. J. Dyson and P. E. Wright, *Curr. Opin. Struct. Biol.*, 1993, **3**, 60–65.
47 D. A. Pearlman, *J. Biomol. NMR*, 1994, **4**, 1–16.
48 I. Compañón, A. Guerreiro, V. Mangini, J. Castro-López, M. Escudero-Casao, A. Avenoza, J. H. Busto, S. Castillón, J. Jiménez-Barbero, J. L. Asensio, G. Jiménez-Osés, O. Boutureira, J. M. Peregrina, R. Hurtado-Guerrero, R. Fiammengo, G. J. L. Bernardes and F. Corzana, *J. Am. Chem. Soc.*, 2019, **141**, 4063–4072.
49 D. A. Case, S. R. Brozell, D. S. Cerutti, T. E. Cheatham III, V. W. D. Cruzeiro, T. A. Darden, R. E. Duke, D. Ghoreishi, H. Gohlke, A. W. Goetz, D. Greene, R. Harris, N. Homeyer, S. Izadi, A. Kovalenko, T. S. Lee, S. LeGrand, P. Li, C. Lin, J. Liu, T. Luchko, R. Luo, D. J. Mermelstein, K. M. Merz, Y. Miao, G. Monard, H. Nguyen, I. Omelyan, A. Onufriev, F. Pan, R. Qi, D. R. Roe, A. Roitberg, C. Sagui, S. Schott-Verdugo, J. Shen, C. L. Simmerling, J. Smith, J. Swails, R. C. Walker, J. Wang, H. Wei, R. M. Wolf, X. Wu, L. Xiao, D. M. York and P. A. Kollman, *AMBER 2018*, University of California, San Francisco, 2018.
50 J. A. Maier, C. Martinez, K. Kasavajhala, L. Wickstrom, K. E. Hauser and C. Simmerling, *J. Chem. Theory Comput.*, 2015, **11**, 3696–3713.
51 K. N. Kirschner, A. B. Yongye, S. M. Tschampel, J. González-Outeiriño, C. R. Daniels, B. L. Foley and R. J. Woods, *J. Comput. Chem.*, 2008, **29**, 622–655.
52 J. Wang, R. M. Wolf, J. W. Caldwell, P. A. Kollman and D. A. Case, *J. Comput. Chem.*, 2004, **25**, 1157–1174.
53 F. Corzana, J. H. Busto, G. Jiménez-Osés, M. García de Luis, J. L. Asensio, J. Jiménez-Barbero, J. M. Peregrina and A. Avenoza, *J. Am. Chem. Soc.*, 2007, **129**, 9458–9467.
54 I. A. Bermejo, I. Usabiaga, I. Compañón, J. Castro-López, A. Insausti, J. A. Fernández, A. Avenoza, J. H. Busto, J. Jiménez-Barbero, J. L. Asensio, J. M. Peregrina, G. Jiménez-Osés, R. Hurtado-Guerrero, E. J. Cocinero and F. Corzana, *J. Am. Chem. Soc.*, 2018, **140**, 9952–9960.
55 N. Martínez-Sáez, J. Castro-López, J. Valero-González, D. Madariaga, I. Compañón, V. J. Somovilla, M. Salvadó, J. L. Asensio, J. Jiménez-Barbero, A. Avenoza, J. H. Busto, G. J. L. Bernardes, J. M. Peregrina, R. Hurtado-Guerrero and F. Corzana, *Angew. Chem., Int. Ed.*, 2015, **54**, 9830–9834.
56 A. García-Herrero, E. Montero, J. L. Muñoz, J. F. Espinosa, A. Vián, J. L. García, J. L. Asensio, F. J. Cañada and J. Jiménez-Barbero, *J. Am. Chem. Soc.*, 2002, **124**, 4804–4810.
57 L. Cipolla, F. Peri and C. Airoldi, *Adv. Anticancer Agents Med. Chem.*, 2008, **8**, 92–121.
58 A. Kaiser, N. Gaidzik, U. Westerlind, D. Kowalczyk, A. Hobel, E. Schmitt and H. Kunz, *Angew. Chem., Int. Ed.*, 2009, **48**, 7551–7555.
59 V. Lakshminarayanan, P. Thompson, M. A. Wolfert, T. Buskas, J. M. Bradley, L. B. Pathangey, C. S. Madsen, P. A. Cohen, S. J. Gendler and G.-J. Boons, *Proc. Natl. Acad. Sci. U. S. A.*, 2012, **109**, 261–266.
60 F. Nimmerjahn and J. V Ravetch, *Science*, 2005, **310**, 1510–1512.
61 N. Martínez-Sáez, N. T. Supekar, M. A. Wolfert, I. A. Bermejo, R. Hurtado-Guerrero, J. L. Asensio, J. Jiménez-Barbero, J. H. Busto, A. Avenoza, G.-J. Boons, J. M. Peregrina and F. Corzana, *Chem. Sci.*, 2016, **7**, 2294–2301.
62 C. Plattner, M. Höfener and N. Sewald, *Org. Lett.*, 2011, **13**, 545–547.
63 V. J. Somovilla, I. A. Bermejo, I. S. Albuquerque, N. Martínez-Sáez, J. Castro-López, F. García-Martín, I. Compañón, H. Hinou, S.-I. Nishimura, J. Jiménez-Barbero, J. L. Asensio, A. Avenoza, J. H. Busto, R. Hurtado-Guerrero, J. M. Peregrina, G. J. L. Bernardes and F. Corzana, *J. Am. Chem. Soc.*, 2017, **139**, 18255–18261.
64 C. I. Bayly, P. Cieplak, W. Cornell and P. A. Kollman, *J. Phys. Chem.*, 1993, **97**, 10269–10280.
65 M. J. Frisch, G. W. Trucks, H. B. Schlegel, G. E. Scuseria, M. A. Robb, J. R. Cheeseman, G. Scalmani, V. Barone, G. A. Petersson, H. Nakatsuji, X. Li, M. Caricato, A. V. Marenich, J. Bloino, B. G. Janesko, R. Gomperts, B. Mennucci, H. P. Hratchian, J. V. Ortiz, A. F. Izmaylov, J. L. Sonnenberg, D. Williams-Young, F. Ding, F. Lipparini, F. Egidi, J. Goings, B. Peng, A. Petrone, T. Henderson, D. Ranasinghe, V. G. Zakrzewski, J. Gao, N. Rega, G. Zheng, W. Liang, M. Hada, M. Ehara, K. Toyota, R. Fukuda, J. Hasegawa, M. Ishida, T. Nakajima, Y. Honda, O. Kitao, H. Nakai, T. Vreven, K. Throssell, J. A. Montgomery Jr., J. E. Peralta, F. Ogliaro, M. J. Bearpark, J. J. Heyd, E. N. Brothers, K. N. Kudin, V. N. Staroverov, T. A. Keith, R. Kobayashi, J. Normand, K. Raghavachari, A. P. Rendell, J. C. Burant, S. S. Iyengar, J. Tomasi, M. Cossi, J. M. Millam, M. Klene, C. Adamo, R. Cammi, J. W. Ochterski, R. L. Martin, K. Morokuma, O. Farkas, J. B. Foresman and D. J. Fox, *Gaussian 16, Revision C.01*, Gaussian, Inc., Wallingford CT, 2016.
66 W. L. Jorgensen, J. Chandrasekhar, J. D. Madura, R. W. Impey and M. L. Klein, *J. Chem. Phys.*, 1983, **79**, 926–935.
67 T. Darden, D. York and L. Pedersen, *J. Chem. Phys.*, 1993, **98**, 10089–10092.
68 W. Kabsch, *Acta Crystallogr., Sect. D: Biol. Crystallogr.*, 2010, **66**, 125–132.
69 M. D. Winn, C. C. Ballard, K. D. Cowtan, E. J. Dodson, P. Emsley, P. R. Evans, R. M. Keegan, E. B. Krissinel, A. G. W. Leslie, A. McCoy, S. J. McNicholas, G. N. Murshudov, N. S. Pannu, E. A. Potterton, H. R. Powell, R. J. Read, A. Vagin and K. S. Wilson, *Acta Crystallogr., Sect. D: Biol. Crystallogr.*, 2011, **67**, 235–242.
70 N. 4 Collaborative Computational Project, *Acta Crystallogr., Sect. D: Biol. Crystallogr.*, 1994, **50**, 760–763.
71 P. Emsley and K. Cowtan, *Acta Crystallogr., Sect. D: Biol. Crystallogr.*, 2004, **60**, 2126–2132.
72 G. N. Murshudov, P. Skubák, A. A. Lebedev, N. S. Pannu, R. A. Steiner, R. A. Nicholls, M. D. Winn, F. Long and A. A. Vagin, *Acta Crystallogr., Sect. D: Biol. Crystallogr.*, 2011, **67**, 355–367.
73 R. A. Laskowski, M. W. MacArthur, D. S. Moss and J. M. Thornton, *J. Appl. Crystallogr.*, 1993, **26**, 283–291.
74 J. K. Gathuru, F. Koide, G. Ragupathi, J. L. Adams, R. T. Kerns, T. P. Coleman and P. O. Livingston, *Vaccine*, 2005, **23**, 4727–4733.

